J. Fluid Mech. (1978), *vol.* 88, *part* 4, *pp.* 769–792
Printed in Great Britain

Convection fluid dynamics in a model of a fault zone in the earth's crust

By D. R. KASSOY AND A. ZEBIB†
Department of Mechanical Engineering, University of Colorado, Boulder

(Received 15 April 1977 and in revised form 3 April 1978)

Faulted regions associated with geothermal areas are assumed to be composed of rock which has been heavily fractured within the fault zone by continuous tectonic activity. The fractured zone is modelled as a vertical, slender, two-dimensional channel of saturated porous material with impermeable walls on which the temperature increases linearly with depth. The development of an isothermal slug flow entering the fault at a large depth is examined. An entry solution and the subsequent approach to the fully developed configuration are obtained for large Rayleigh number flow. The former is characterized by growing thermal boundary layers adjacent to the walls and a slightly accelerated isothermal core flow. Further downstream the development is described by a parabolic system. It is shown that a class of fully developed solutions is not spatially stable.

1. Introduction

A study of the fluid dynamics within a geothermal system should consider a physically viable conceptual model based on geophysical and geological evidence and interpretation. The fluid mechanician can then translate this model into governing equations and boundary conditions for which solutions can be developed.

In this paper a study is made of the convection of liquid in a particular type of hydrothermal system which is found fairly frequently within the first few kilometres of the earth's crust. In order to provide a sound physical foundation for the analysis to follow, this introduction contains a discussion of the pertinent geological and geophysical considerations. This information is then used to construct a mathematical system capable of describing convection and heat transfer in a conceptual model of a vertical fault zone. The analysis is carried out in terms of liquid flowing in a slender, vertical, two-dimensional channel filled with a porous medium. The channel is charged with heated liquid from below which rises owing to buoyant effects. The nature of the developing flow pattern and the heat-transfer distribution is elucidated by means of a high Rayleigh number asymptotic analysis which is an adaptation of Van Dyke's (1970) ideas.

1.1. *The physical environment*

The heat- and mass-transfer processes in a liquid-dominated geothermal anomaly depend upon the detailed geological structure of the system and the nature of the hydrodynamic convection process occurring within that physical environment. When

† Permanent address: Mechanical Engineering Department, Rutgers University, New Brunswick, New Jersey.

the geological structure is relatively uniform in nature, the hydrodynamical patterns themselves will tend to determine the distribution of physical properties (temperature, pressure, velocity) characterizing the system. Conversely, the upwelling of hot liquid in anomalies closely associated with localized geological structures like faulted regions and narrowly defined aquifers appears to be strongly influenced by the detailed structural features (Ellis 1975).

Recent studies of liquid-dominated systems suggest that many geothermal anomalies are intimately associated with specific patterns of faulting. In the Wairakei field it appears that heated water rises from a large depth along the active Waiora and Wairakei faults to charge the Waiora aquifer (Grindley 1965). The production of geothermal fluids from bore holes in the Broadlands region is most prolific where there are faults that transect the rhyolite dome that caps the Waiora formation (Grindley 1970). Prior to production at Cerro Prieto, vigorous hot springs existed along a linear surface feature (Mercado 1969). Rinehart & Ross (1964) and Bailey, Dalrymple & Lanphere (1976) have noted that most of the active hot springs and fumeroles in Long Valley, California occur along active north-to-northwest tending faults. It has also been suggested by Bailey *et al.* (1976) that the dominant controlling structures of the hydrothermal activity are the deep caldera ring fractures. In the Imperial Valley, California there are several geothermal anomalies which are close to or intersected by active faults (Elders, Rex & Meidav 1972). Swanberg (1974, 1976), Black (1975) and Bailey (1977) have concluded that the East Mesa anomaly in the Imperial Valley exists because heated fluid can rise from a large depth along faults which are known from remote sensing and microearthquake monitoring (Combs & Hadley 1977). Geothermal activity also appears to be associated with the Imperial fault at the Alamo anomaly in the Imperial Valley (Swanberg 1974).

Since there is a reasonable body of circumstantial evidence suggesting that faulted regions are frequently associated with geothermal systems, it is of value to ask what role the fault plays in determining the hydrological and thermodynamic state of the area. The answer must be somewhat speculative because the available bore-hole data from geothermal fields is limited and because little is known about the detailed structure of fault regions, particularly at larger depths (Wu, Blatter & Robertson 1975). Since the water in geothermal systems appears to be largely of meteoric origin (White 1961; Ellis 1975) it may be hypothesized that surface water gradually percolates down into permeable sediments and/or fractured volcanic rock. The area of downflow is thought to be considerably larger than the thermal anomaly itself. At depth the water is close to the local heat source. It is buoyant relative to the cool surrounding recharge water. If a faulted region is present, then the heated water can rise in this region of relatively large vertical permeability, convecting energy towards the surface. When the fault intersects horizontal aquifers of relatively large permeability the rising hot water will charge the aquifer.

The fault itself is hypothesized to be a region of heavily fractured material of finite width bounded by two vertical planes. The vertical extent of the fault and its second horizontal dimension are large compared with its width. Often the fault has been active for extensive periods because the region exhibits volcanism and/or tectonic events (Elders *et al.* 1972). The continual microearthquake activity frequently associated with fault-controlled geothermal systems (Combs & Hadley 1977; Ward 1972) suggests that there are mechanical processes available for fracturing of the rock.

This is necessary to counteract the mineral deposition associated with a rising, cooling column of saline geothermal fluid, which tends to close up the system by reducing the permeability (Ellis 1975). The epicentres of the microearthquakes associated with the East Mesa anomaly are frequently deeper than the presumed local basement depth of the Imperial Valley. Thus one may speculate that the fault extends through the sediments of the graben into the basement rock of magmatic origin beneath.

The near-surface distribution of heat transfer at a geothermal anomaly associated with a fault zone (e.g. Combs 1971) is related in part to the nature of the convective flow in that fault. Hence it appears useful to develop models of the fluid flow in a faulted region. One could proceed by considering flow in a complex pattern of discrete intersecting fractures. However, given the lack of information about the fault-zone structure, in particular fracture distribution, this approach does not appear to be particularly meaningful. Instead the problem is considered in terms of flow in saturated porous media. In this case the details of the structure appear in the averaged properties of permeability and porosity. The values used for these quantities are those associated with the fracture system, in which most of the fluid flow is presumed to occur, rather than with the intrinsic (intergranular) properties of the rock itself.

2. Modelling

Imagine a vertical fault zone which begins at the surface and extends through a length L' of sedimentary material and a length l' of subsequent basement rock as shown in figure 1. The transverse width $2y'_e \ll L'$ represents the region of extensive fracture distribution associated with the faulting process. Within the sedimentary section the effective permeability of the fault zone is assumed to be large compared with that of the surrounding unfractured rock. The relatively brittle basement-rock complex of depth l' is assumed to be fractured everywhere although most intensively in the fault zone. Below this depth the fracture system is considered to be closed owing to creep deformation of the hot rock system associated with a localized heat source. Water, which has percolated down into the fractured basement complex far from the fault, flows laterally towards the fault as it is heated. The driving mechanism is the hydrostatic pressure imbalance between the peripheral cold recharge region and the hot upflow column in the fault (Donaldson 1970). Since the vertical fracture permeability of the fault is large compared with the general permeability in the neighbouring basement section, the horizontal pressure gradient drives hot liquid into the bottom portion of the fault. Subsequently the fluid moves upwards, cooling as it approaches the surface.

The heat and mass transfer within the fault zone will be modelled by considering the flow in a saturated porous medium contained in the two-dimensional channel shown in figure 2(*a*). When $-L' < z' < 0$, the vertical walls are considered impermeable to emphasize the contrast in permeability between the fault and its surroundings.† In the region $-(L'+l') < z' < -L'$ it is assumed that mass can cross the walls with a velocity $v'_w(z)$ which vanishes at $z' = -L'$ and $z' = -(L'+l')$. This distribution is chosen to provide a smooth transition between the impermeable wall above $z' = -L'$

† A future paper will consider the problem of aquifer charging.

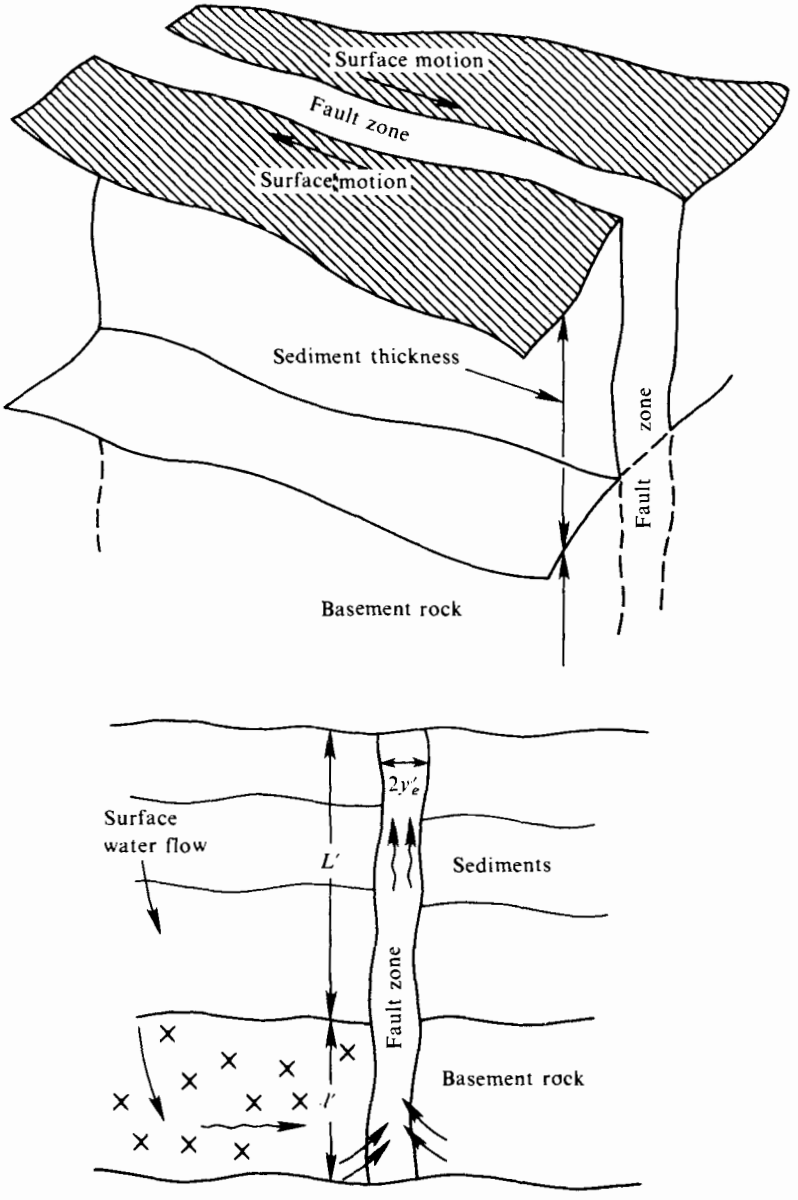

FIGURE 1. A conceptual view of a vertical fault zone extending through sediments of thickness L' and basement rock of magmatic origin.

and below $z' = -(L'+l')$. At $z' = -(L'+l')$ the boundary is considered to be impermeable because of the closed fracture system beneath that depth. Fluid is assumed to leave the channel freely at $z' = 0$. There is a linear temperature increase with depth along the vertical boundary from T'_0 to T'_1 for $-L' < z' < 0$ and a uniform temperature T'_1 below (in $-(L'+l') < z' < -L'$). While the latter condition is not entirely correct from the observational viewpoint, it permits one to consider an isothermal fault *charging* process followed by a thermally active problem involving the cooling of a

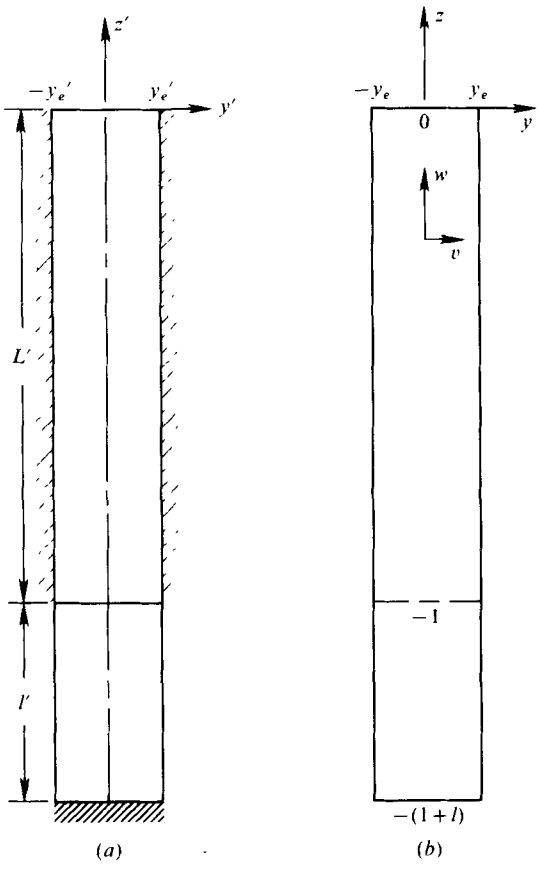

FIGURE 2. (*a*) Dimensional and (*b*) non-dimensional view of the vertical slot filled with a saturated porous medium.

rising column of relatively hot fluid. The precise form of the boundary conditions permits mathematical simplifications which lead to analytical solution development.

In order to simplify the analysis further, it is assumed that the decrease in the liquid viscosity (μ') with depth (associated with increasing temperature) is matched by an analogous decrease in the permeability (k') due to compaction. As a result the ratio μ'/k' is a constant.

The non-dimensional governing equations can be written in the form

$$v_y + w_z = 0, \tag{1}$$

$$v = -p_y, \quad w = -p_z + (T-1)/\tau, \tag{2a,b}$$

$$R\,[vT_y + wT_z] = T_{yy} + T_{zz}. \tag{3}$$

The volumetric velocity components v and w, the pressure p, the temperature T, the lengths y and z, the overheat parameter τ and the Rayleigh number R are defined with respect to dimensional (primed) quantities by

$$v = \frac{v'}{q_R'}, \quad w = \frac{w'}{q_R'}, \quad q_R' = \frac{g' k_0' \alpha' \Delta T'}{\nu_0'}, \tag{4a,b,c}$$

$$p = \frac{p' - \rho_0' g' z'}{P_R'}, \quad p_R' = \rho_0' g' L' \alpha' \Delta T', \quad T = \frac{T'}{T_0'}, \tag{4d,e,f}$$

$$y = \frac{y'}{L'}, \quad z = \frac{z'}{L'}, \quad \tau = \frac{T_1' - T_0'}{T_0'}, \tag{4g,h,i}$$

$$R = \frac{g' k_0' \alpha' L' \Delta T'}{\nu_0'^2} Pr_m. \tag{4j}$$

Here g' is the acceleration due to gravity, k' is the permeability, α' is the constant thermal expansion coefficient, $\Delta T' = T_1' - T_0'$, ν' is the kinematic viscosity of water, ρ' is the density of water, Pr_m is the Prandtl number based on the conductivity of the saturated medium and the subscript zero refers to conditions at $z' = 0$. The non-dimensional configuration is shown in figure 2(*b*).

The associated boundary conditions can be described by

$$v(z, \pm y_e) = 0, \quad T(z, \pm y_e) = 1 - \tau z \quad \text{for} \quad -1 \leqslant z \leqslant 0, \tag{5a,b}$$

$$v(z, \pm y_e) = \mp v_w(z), \quad T(z, \pm y_e) = 1 + \tau \quad \text{for} \quad -(1+l) < z < -1, \tag{5c,d}$$

$$w_z(0, y) = 0, \quad w(-(1+l), y) = 0 \quad \text{for} \quad -y_e \leqslant y \leqslant y_e. \tag{5e,f}$$

In the region where the walls are impermeable the non-dimensional mass flux can be written as

$$M = \frac{1}{2y_e} \int_{-y_e}^{+y_e} w \, dy \equiv \frac{m'}{2y_e' q_R' \rho_0'}. \tag{6}$$

The quantity m' is a measure of the mass entering the fault zone at $z = -1$. The problem's solution is parametrically dependent upon this quantity, which cannot be specified without a complete analysis of the entire circulation pattern of the water (including the downflow into the basement rock and the horizontal transit process during which the liquid is heated). From the viewpoint of the present theory m' must be found *a posteriori* from a comparison of solutions with appropriate field or experimental measurements.

The explicit form of $v_w(z)$ is chosen to be

$$v_w(z) = 4 v_M l^{-2} (-z - 1)[z + (1 + l)], \tag{7}$$

in which v_M, the maximum velocity, occurs at $z = z_M = -(1 + \frac{1}{2}l)$.

Solutions for the system (1)–(7) are sought for specified values of τ, R, y_e and M. From the physical viewpoint it is of interest to consider $R \gg 1$ ($R = 10^2$–10^3) and $y_e \ll 1$ such that $Ry_e^2 = O(1)$. In this case Ry_e, which is the Rayleigh number based on the channel half-width, is a large quantity.

3. Isothermal charging of the fault zone

In the lower portion of the fault, $-(1+l) \leqslant z < -1$, the boundary condition (5*d*) implies an isothermal flow. It follows from (1)–(3), (5*c*) and the appropriate scalings $y = y_e \bar{y}$ and $v = y_e \bar{v}$ that the basic system can be written as

$$\bar{v}_{\bar{y}} + w_z = 0, \quad p_{\bar{y}} = -y_e^2 \bar{v}, \quad w = -p_z + 1,$$

$$\bar{v}(z, \pm 1) = \mp v_w(z)/y_e, \quad w(-(1+l), \bar{y}) = 0.$$

If we consider the asymptotic limit $y_e \to 0$ with $\bar{y}$ and z fixed, then the basic solution is

$$w_0 = M\left[1 - \frac{3(1+z)^2}{l^2} - \frac{2(1+z)^3}{l^3}\right], \quad v_0 = y_e \bar{v}_0 = -v_w(z)\bar{y}, \tag{8a,b}$$

$$M = (\tfrac{2}{3}) v_M l / y_e, \quad T = 1 + \tau. \tag{9a,b}$$

The corrections to w and v are $O(y_e^2)$ and $O(y_e^3)$ respectively. An $O(1)$ mass flux M is obtained if $v_M = O(y_e)$. It follows from (8*b*) that $v \ll w$ since $\bar{y} = O(1)$. The axial velocity is essentially a slug-type flow which increases in magnitude as mass is added at the boundary. As the point $z = -1$ is approached from below $w \to M$ and $v \to 0$. Formally (8) and (9) are correct only for $z < -1$ because the change in boundary conditions at $z = -1$, described in (5*a–d*), is associated with a weak upstream effect which will be considered in detail.

4. The thermally active fault-zone flow

It is now required to determine how the isothermal slug flow at $z = -1^-$ is altered as the rising column of fluid is cooled. The fluid entering the thermally active region with a temperature $T = 1 + \tau$ will be cooled at the walls as a result of the boundary condition (5*b*). Since the tube Rayleigh number Ry_e is large, the thermal cooling layer will be small compared with y_e. In the thin layer the temperature will be less than that in the adjacent isothermal core. It follows from (2*b*) that the buoyancy force is reduced and hence the fluid velocity will be less than the initial value. The core velocity must then increase slightly to account for the reduced mass carried in the thin thermal layers. In this way, the physical description of the entry-length development of the temperature and velocity profiles can be rationalized.

Sufficiently far downstream, when the growing thermal wall layers fill a large portion of the tube, the flow configuration will be dramatically different from the initial conditions. The development further downstream in this channel of small aspect ratio involves the approach towards the fully developed solution in which the axial velocity is a function of only the transverse variable.

The mathematical approach for modelling the flow is an adaptation of the ideas presented by Van Dyke (1970) for studying entry flow of an incompressible viscous fluid in a channel, a purely isothermal problem involving the development of a parabolic Poiseuille profile. Unlike that problem, in which the developmental aspects are associated with the growth of thin viscous boundary layers near the wall, the present consideration must be focused on the influence of the thermal properties of the flow. It should also be stressed that the entry region considered here involves development from a previously well-defined isothermal channel flow. This is in contrast to Van Dyke's cascade problem, in which the appropriate upstream boundary condition is a uniform flow 'far' from the entry point.

5. Entry flow

The stream-function form of (1)–(3), (5*a*, *b*) and (6) can be written as

$$\nabla^2 \Psi = \frac{T_y}{\tau}, \quad \nabla^2 = \frac{\partial^2}{\partial z^2} + \frac{\partial^2}{\partial y^2}, \tag{10}$$

$$R[\Psi_y T_z - \Psi_z T_y] = \nabla^2 T, \tag{11}$$

$$T(z, \pm y_e) = 1 - \tau z, \quad \Psi_z(z, \pm y_e) = 0, \tag{12a, b}$$

$$M = (2y_e)^{-1}[\Psi(z, y_e) - \Psi(z, -y_e)], \tag{13}$$

where $w = \Psi_y$ and $v = -\Psi_z$. Just upstream of the entry point $z = -1$,

$$\Psi(-1^-, y) = My, \quad T(-1^-, y) = 1+\tau. \tag{14}$$

Asymptotic solutions will be sought in the limit $y_e \ll 1$ such that $\gamma \equiv R^{\frac{1}{2}} y_e = O(1)$.

In the entry region, where the length scale is y_e, the appropriately scaled variables

$$\bar{z} = (1+z)/y_e, \quad \bar{y} = y/y_e, \quad \bar{\Psi} = \Psi/y_e \tag{15a,b,c}$$

can be used in (10)–(14) to obtain

$$\bar{\nabla}^2 \bar{\Psi} = T_{\bar{y}}/\tau, \tag{16}$$

$$\gamma^2 [\bar{\Psi}_{\bar{y}} T_{\bar{z}} - \bar{\Psi}_{\bar{z}} T_{\bar{y}}] = y_e \bar{\nabla}^2 T, \tag{17}$$

$$T(\bar{z}, \pm 1) = 1+\tau-y_e \tau \bar{z}, \quad \bar{\Psi}_{\bar{z}}(\bar{z}, \pm 1) = 0, \tag{18a,b}$$

$$M = \tfrac{1}{2}[\bar{\Psi}(\bar{z}, 1) - \bar{\Psi}(\bar{z}, -1)], \tag{19}$$

$$\bar{\Psi}(\bar{z} \to -\infty, \bar{y}) = M\bar{y}, \quad T(\bar{z} \to -\infty, \bar{y}) = 1+\tau, \tag{20a,b}$$

where $\bar{\nabla}^2$ is the operator in (10) with y and z replaced by barred quantities. In the limit $y_e \to 0$, (17) reduces to a statement that the convective operator is zero. Since the velocity is non-zero, it follows that $T \approx 1+\tau$, which is clearly representative of the adiabatic core away from the walls. To a first approximation (16) reduces to a Laplace equation for $\bar{\Psi}$ which must satisfy (18b) and (20a). Thus the slug flow prevails; $\bar{\Psi} \approx M\bar{y}$. These solutions are not valid adjacent to the wall, where a boundary layer must exist. The fuller core expansions can be written as

$$\bar{\Psi} \sim M\bar{y} + y_e^{\frac{3}{2}} \bar{\Psi}_1(\bar{z}, \bar{y}) + \ldots, \tag{21}$$

$$T \sim 1+\tau+EST(y_e). \tag{22}$$

The corrections in (21) and (22) result from thermal-boundary-layer effects which are to be discussed. The term $EST(y_e)$ in (22) denotes terms which are exponentially small with respect to the parameter.

The thermal-boundary-layer transverse variable, found by rescaling (17) such that there is an inherent balance between conduction and convection in the energy equation when $y_e \to 0$, has the form

$$Y = (1-\bar{y})/y_e^{\frac{1}{2}}$$

near the wall $\bar{y} = 1$. The geometric configuration is shown in figure 3. Asymptotic expansions can be written as

$$\bar{\Psi} \sim M(1-y_e^{\frac{1}{2}} Y) + y_e^{\frac{3}{2}} F(\bar{z}, Y), \tag{23}$$

$$T \sim 1+\tau-y_e H(\bar{z}, Y). \tag{24}$$

It is observed that the $O(y_e^{\frac{3}{2}})$ term in (23) represents a weak correction to the core stream function. The disturbance is small because the no-slip condition cannot be considered within the context of the porous-media equations. In (24) the correction represents the basic cooled thermal boundary layer. In the lowest-order approximation the equations for F and H, as derived from (16), (17) and (22)–(24), can be written as

$$F_{0YY} = H_{0Y}/\tau, \quad aH_{0\bar{z}} = H_{0YY}, \quad a = \gamma^2 M. \tag{25a,b,c}$$

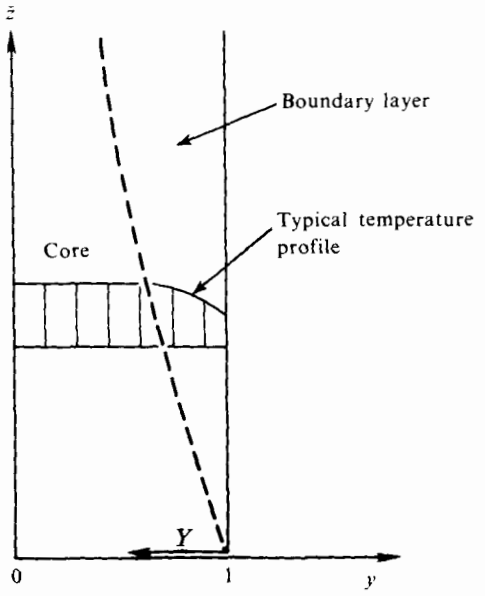

FIGURE 3. The entry-flow plane and variables.

The conditions to be met by the solutions, obtained from (12) and by constructing matching criteria with the core, have the form

$$F_{0\bar{z}}(\bar{z}, 0) = 0, \quad F_{0Y}(\bar{z}, Y \to \infty) = 0, \tag{26a,b}$$

$$H_0(\bar{z}, 0) = \tau\bar{z}, \quad H_0(\bar{z}, Y \to \infty) = 0. \tag{26c,d}$$

In terms of classical functions (Abramowitz & Stegun 1965, p. 297) the solutions can be written as

$$F_0 = \left(\frac{2}{a}\right)^{\frac{1}{2}} \bar{z}^{\frac{3}{2}} \left\{\left(\eta + \frac{\eta^3}{3}\right) \operatorname{erfc}\left(\frac{\eta}{\sqrt{2}}\right) + \frac{2}{3}\left(\frac{2}{\pi}\right)^{\frac{1}{2}} \left[1 - \left(1 + \frac{\eta^2}{2}\right) \exp\left(-\frac{\eta^2}{2}\right)\right]\right\}, \tag{27}$$

$$H_0 = \tau\bar{z}\left[(1+\eta^2) \operatorname{erfc}\left(\frac{\eta}{\sqrt{2}}\right) - \left(\frac{2}{\pi}\right)^{\frac{1}{2}} \eta \exp\left(-\frac{\eta^2}{2}\right)\right], \tag{28}$$

$$\eta = \left(\frac{a}{2}\right)^{\frac{1}{2}} Y(\bar{z})^{-\frac{1}{2}}. \tag{29}$$

From (23), (24) and (27)–(29) one may ascertain that at the wall ($\bar{y} = 1$)

$$w = M - y_e\bar{z}, \quad w_{\bar{y}} = -y_e^{\frac{1}{2}} 2\left(\frac{a\bar{z}}{\pi}\right)^{\frac{1}{2}} = \frac{1}{\tau}\frac{\partial T}{\partial \bar{y}}. \tag{30a,b}$$

The initial slip velocity M is reduced with increases in $\bar{z}$ while the wall shear and heat transfer (in effect) increase.

By considering the limit $Y \to \infty$ with $\bar{z}$ fixed it is possible to show that at the outer edge of the boundary layer

$$H_0 = O\left[Y^{-3} \exp\left(-\frac{a}{2}\frac{Y^2}{\bar{z}}\right)\right],$$

which helps to justify (22). The same limit can be used to show that, for the boundary layer at $\bar{y} = 1$,

$$v(\bar{z}, Y \to \infty) \sim -y_e^{\frac{3}{2}} 2\left(\frac{\bar{z}}{a\pi}\right)^{\frac{1}{2}}, \tag{31}$$

which verifies (21). This means that the displacement effect of the thermally induced boundary layer acts on the core flow like a surface distribution of sources in a manner similar to that seen in a viscous momentum boundary layer (Van Dyke 1964, p. 134, 1970).

If the limit $\bar{z} \to \infty$ with η fixed is taken in (23), (24) and (27)–(29) it is found that the boundary-layer expansions are invalid when $\bar{z} = O(1/y_e)$, which corresponds to $z = O(1)$ and $\bar{y} = O(1)$. In that region further development of the flow takes place.

The core correction $\bar{\Psi}_1$ can now be obtained from the system

$$\nabla^2 \bar{\Psi}_1 = 0, \tag{32}$$

$$\bar{\Psi}_{1\bar{x}}(\bar{z}, \pm 1) = \pm 2(\bar{z}/a\pi)^{\frac{1}{2}} \quad \text{for} \quad \bar{z} > 0, \tag{33}$$

$$\bar{\Psi}_1(\bar{z}, \pm 1) = 0 \quad \text{for} \quad \bar{z} < 0, \tag{34}$$

$$\bar{\Psi}_1(\bar{z} \to -\infty, \bar{y}) = 0. \tag{35}$$

Equation (32) is obtained from the limiting forms of (16), (17), (21) and (22). The effective source condition in (33) obtained from (31) is derived formally by matching the wall boundary layers and the core region. Equations (34) and (35) are boundary conditions on the flow upstream of $\bar{z} = 0$ in a region of extent $O(y_e)$ measured on the z scale. It is to be noted that the basic charging solution described in $(8a, b)$ has the form

$$w = M + O(y_e^2), \quad v = O(y_e^2) \tag{36}$$

in the region $O(y_e)$ upstream of entry. The corrections to the slug flow $w = M, v = 0$ are smaller than the correction $\bar{\Psi}_1$ induced by the thermal-boundary-layer phenomena. Hence the latter must decay for $\bar{z} \to -\infty$. The solution to (32)–(35) describes the upstream influence of the thermal effects as well as the acceleration of the core for $\bar{z} > 0$. For present purposes it is of interest to obtain the asymptotic form of $\bar{\Psi}_1$ far downstream. An asymptotic analysis can be used to show that

$$\bar{\Psi}_1(\bar{z} \to \infty, \bar{y}) \sim \frac{4\bar{z}^{\frac{3}{2}}}{3(a\pi)^{\frac{1}{2}}} \left[\bar{y} + \frac{\bar{y} - \bar{y}^3}{8\bar{z}^2} + \ldots\right], \tag{37}$$

from which it follows that

$$w(\bar{z} \to \infty, \bar{y}) \sim M + y_e^{\frac{3}{2}} \frac{4(\bar{z})^{\frac{3}{2}}}{3(a\pi)^{\frac{1}{2}}} \left[1 + \frac{1 - 3\bar{y}^2}{8\bar{z}^2} + \ldots\right]. \tag{38}$$

The first term in the correction represents the basic acceleration of the core. It may be observed from (38) that when the non-uniformity occurs $[\bar{z} = O(1/y_e)]$ the correction is $O(1)$. Hence the core is substantially altered from the initial slug-flow profile. It is to be noted that the temperature remains isothermal because of the exponential decay property of the thermal boundary layer.

6. Downstream flow

The non-uniformity in the entry-flow expansions implies that the appropriate downstream variables are z and $\bar{y}$. If $(15b, c)$ are used in (10)–(12) it follows that

$$\tilde{\Psi}_{\bar{y}\bar{y}} + y_e^2 \tilde{\Psi}_{zz} = \tilde{T}_{\bar{y}}/\tau, \tag{39}$$

$$\gamma^2 [\tilde{\Psi}_{\bar{y}} \tilde{T}_z - \tilde{\Psi}_z \tilde{T}_{\bar{y}}] = \tilde{T}_{\bar{y}\bar{y}} + y_e^2 \tilde{T}_{zz}, \tag{40}$$

$$\tilde{\Psi}_z(z, \pm 1) = 0, \quad \tilde{T}(z, \pm 1) = 1 - \tau z. \tag{41a, b}$$

The initial conditions for this system, obtained by matching the downstream region with the asymptotic extent of the entry flow, are

$$\tilde{\Psi}(z \to -1^+, \bar{y}) \sim \left(M\bar{y} + \frac{4}{3(a\pi)^{\frac{1}{2}}}(1+z)^{\frac{3}{2}}\bar{y} + O([1+z]^2)\right) + O(y_e^2), \tag{42}$$

$$\tilde{T}(z \to -1^+, \bar{y}) \sim (1+\tau) + EST(y_e). \tag{43}$$

The first-order approximations to $\tilde{\Psi}$ and $\tilde{T}$ are described by the reduced form of (39)–(43) obtained from the limit $y_e \to 0$:

$$\tilde{\Psi}_{0\bar{y}\bar{y}} = \tilde{T}_{0\bar{y}}/\tau, \tag{44}$$

$$\gamma^2[\tilde{\Psi}_{0\bar{y}}\tilde{T}_{0z} - \tilde{\Psi}_{0z}\tilde{T}_{0\bar{y}}] = \tilde{T}_{0\bar{y}\bar{y}}, \tag{45}$$

$$\Psi_{0z}(z, \pm 1) = 0, \quad \tilde{T}_0(z, \pm 1) = 1 - \tau z, \tag{46a,b}$$

$$\tilde{\Psi}(-1, \bar{y}) = M\bar{y}, \quad \tilde{T}_0(-1, \bar{y}) = 1 + \tau. \tag{47a,b}$$

Equations (44)–(47) represent a nonlinear parabolic system which describes the development of the initial profiles in (47). Although the latter equation may appear obvious, the entry analysis was necessary for a rigorous derivation.

6.1. *Spatial stability*

Prior to developing the full numerical solution, it is of interest to consider the possibility of fully developed solutions to (44)–(46). This matter is examined by assuming that far from the entry, in the sense that $z' \gg y'_e$, the solutions can be represented by

$$\tilde{\Psi} = \tilde{\Psi}_0(\bar{y}) + \tilde{\Psi}_1(z, \bar{y}), \tag{48}$$

$$\tilde{T} = 1 - \tau[z - \theta_0(\bar{y})] + \tau\theta_1(z, \bar{y}), \tag{49}$$

where the corrections denoted by the subscript 1 are assumed to be small with respect to the basic fully developed solution. It follows from (13), (15*c*), (44)–(46), (48) and (49) that the latter is described by

$$\tilde{\Psi}_0'' = \theta_0', \quad -\gamma^2\tilde{\Psi}_0'' = \theta_0'', \tag{50a,b}$$

$$\tilde{\Psi}_0(1) - \tilde{\Psi}_0(-1) = 2M, \quad \theta_0(\pm 1) = 0, \tag{51a,b}$$

where primes denote derivatives with respect to $\bar{y}$. Equation (51*a*) is a statement of global mass conservation which replaces the initial condition of the full parabolic system. The solution

$$\tilde{\Psi}_0 = \frac{M\sin\gamma\bar{y}}{\sin\gamma}, \quad \theta_0 = \frac{M\gamma}{\sin\gamma}[\cos\gamma\bar{y} - \cos\gamma] \tag{52a,b}$$

is valid for $\gamma \neq n\pi$ ($n = 1, 2, 3, \ldots$). Axial velocity profiles $w(\bar{y})$ are shown in figure 4 for several values of γ. Symmetric, purely upflow profiles appear for $0 < \gamma \leqslant \frac{1}{2}\pi$. When $\frac{1}{2}\pi < \gamma < \pi$ there are regions of downflow adjacent to the walls. When $\gamma \to \pi^-$, $|w| \to \infty$ while the axial velocity profile implies the existence of nearly equal upward and downward mass flux, so that the throughput remains finite. When $\gamma = \pi$ an additional eigenfunction $\cos\pi\bar{y}$ appears in (52*a*). In terms of the axial velocity the solution is composed of symmetric and antisymmetric modes each of which involve only zero net mass flux. These are representative of the eigenfunctions which can be derived for the onset of convection in the fully developed portion of the long narrow channel

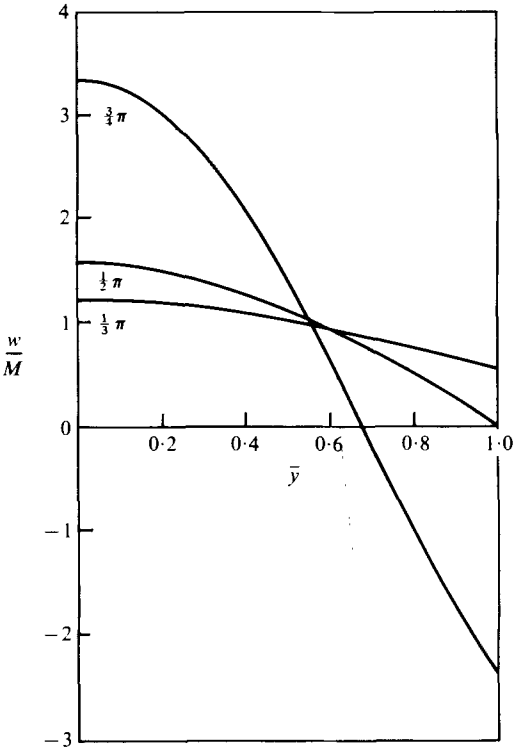

FIGURE 4. Fully developed vertical flow profiles in the slot for $\gamma = \frac{1}{3}\pi$, $\frac{1}{2}\pi$ and $\frac{3}{4}\pi$.

by adopting the ideas of Ostrumov (1946, see Landau & Lifshitz 1959, p. 215). The appearance of reversed flow in the fully developed solutions for $\gamma > \frac{1}{2}\pi$ and large velocities for $\gamma \to \pi^-$ presents conceptual difficulties in the understanding of the development of the slug-flow profile at $z = -1$. How can a flow governed by a parabolic system develop reversed flow? What is the physical mechanism which generates large values of w? Are these flows physically acceptable? An answer to the last question can be obtained by examining the spatial stability of the fully developed profile. We ask whether small corrections to the latter, represented by $\tilde{\Psi}_1$ and θ_1, decay or grow with increasing downstream distance.

The governing equations can be written in the form

$$\tilde{\Psi}_{1\bar{y}\bar{y}} = \theta_{1\bar{y}}, \quad \tilde{\Psi}_{1z}(z, \pm 1) = \theta_1(z, \pm 1) = 0, \tag{53a,b}$$

$$\gamma^2[\tilde{\Psi}_0\theta_{1z} - \tilde{\Psi}_{1\bar{y}} - \theta_0'\tilde{\Psi}_{1z}] = \theta_{1\bar{y}\bar{y}}, \quad \tilde{\Psi}_1(z, 1) = \tilde{\Psi}_1(z, -1). \tag{54a,b}$$

Equations (53a) and (54a) can be combined to produce a fourth-order linear partial differential equation for $\tilde{\Psi}_1$. The solution which satisfies (53b) and (54b) can be written formally in the separable form

$$\tilde{\Psi}_1 \sim e^{-\lambda z} v(\bar{y}), \tag{55}$$

where v is an odd function described by

$$(\cos r)\, v^{\mathrm{iv}} + (\sin r)\, v''' + (\cos r)\, v'' + (\sin r)\, v' + \hat{\lambda}[(\cos^2 r)\, v'' + (\cos r)(\sin r)\, v' + v] = 0, \tag{56}$$

$$v(\pm\gamma) = (v''' + v')(\pm\gamma) = 0, \tag{57a,b}$$

$$r = \gamma\bar{y}, \quad \hat{\lambda} = \gamma M\lambda/\sin\gamma, \quad 0 < \gamma < \pi. \tag{58a,b}$$

This is a non-self-adjoint eigenvalue problem. When $0 < \gamma < \frac{1}{2}\pi$ the system is non-singular. However for $\frac{1}{2}\pi \leqslant \gamma < \pi$ the coefficient of the highest-order derivative is zero somewhere in the field, rendering the problem singular. There are several properties of (56) which can be developed by elementary analysis. For all γ and $\hat{\lambda}$ the even function $\cos r$ is a solution of (56) but does not satisfy all the conditions required for an eigenfunction. When $\gamma = \frac{1}{2}\pi$ and $\hat{\lambda} = 0$ the odd function $v = r\cos r$ is an eigenfunction. It follows that the corresponding fully developed profile shown in figure 4 is neutrally stable. This is interpreted to mean, following Chen & Libby (1968), that this profile would not be observed in an experiment because a small disturbance from the fully developed profile would not decay in the downstream direction.

Further properties of the eigenvalue problem can be developed for the case $\hat{\lambda} \neq 0$. A first integral of (56) can be written in the form

$$v''' + v'' + \hat{\lambda}[(\cos r)\, v' + (\sin r)\, v] = \hat{\lambda} A \cos r, \tag{59}$$

in which the integration constant A is associated with the condition

$$v'(\pm\gamma) = A. \tag{60}$$

The function $f \equiv v'' + v'$ can be used in the differentiated form of (59) to show that

$$f'' + \hat{\lambda}\cos r f = -\hat{\lambda} A \sin r. \tag{61}$$

Equation (57*b*) and the condition that v is an odd function lead to

$$f(0) = f'(\gamma) = 0. \tag{62}$$

The v solution can then be found in terms of quadratures of $f(r)$. If the complete boundary conditions in (57) and the oddness condition are to be met it is necessary that

$$\int_0^\gamma f \sin r\, dr = A \sin\gamma. \tag{63}$$

When $A = 0$, numerically obtained eigensolutions of (61) and (62) do not satisfy the integral condition (63). It follows that only the trivial solution $f = 0$ is possible. Given the complete set of conditions on v, this corresponds to the null result $v = 0$. Hence the case $A = 0$ is not physically viable.

With the normalization $A = 1$, which does not affect the problem (56) and (57) originally formulated, two distinct cases can be examined.

Case I: $0 < \gamma \leqslant \frac{1}{2}\pi$, $\hat{\lambda} \neq 0, A = 1$. If (61) is multiplied by the complex conjugate of f and the result is integrated over the field then it follows, after application of the conditions in (62) and (63), that

$$\hat{\lambda}\left(\sin\gamma + \int_0^\gamma \cos r\, |f|^2\, dr\right) = \int_0^\gamma |f'|^2\, dr.$$

One concludes that the eigensolutions are real and $\hat{\lambda} > 0$.

Standard manipulations with (61)–(63) for any two eigenfunctions f_m and f_n can be used to show that

$$\int_0^\gamma \cos r f_m f_n\, dr = -\sin\gamma.$$

This result combined with that in (63) implies that there can be only a single solution f_0 with no internal nodes in $(0, \gamma)$. Then one can adopt the argument of Ince (1956, p. 225) to show that the corresponding eigenvalue $\hat{\lambda}_0$ is the smallest possible.

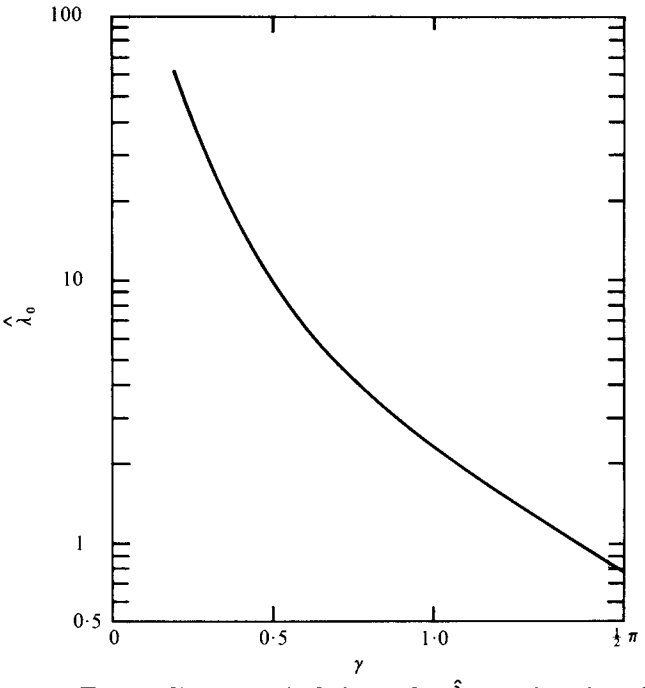

FIGURE 5. The smallest canonical eigenvalue $\hat{\lambda}_0$ as a function of γ for $\gamma \leqslant \frac{1}{2}\pi$.

Numerical solutions to (61)–(63) with $A = 1$ were obtained by using a quasi-linearization technique (Kalaba 1963). In figure 5, the smallest eigenvalue $\hat{\lambda}_0$ is shown as a function of γ. It should be noted from (58*b*) that λ itself also becomes large when $\gamma \ll 1$, which implies [see (55)] that rapid convergence to the fully developed flow is obtained.

As γ increases, corresponding to growth in the conventionally defined channel Rayleigh number Ry_e, the convergence rate becomes less rapid. This implies that for a channel of length L' fully developed flow will not be found for sufficiently large γ. Although not shown on figure 5, the $\hat{\lambda}_0$ curve continues smoothly beyond $\gamma = \frac{1}{2}\pi$. However it is no longer the smallest possible eigenvalue. In particular it should be recalled that when $\gamma = \frac{1}{2}\pi$ there is an eigenvalue corresponding to $\hat{\lambda} = 0$.

Case II: $\frac{1}{2}\pi < \gamma < \pi$, $\hat{\lambda} \neq 0$, $A = 1$. Standard arguments fail in this case because $\cos r$ changes sign at $r = \frac{1}{2}\pi$. However solutions can be constructed by using asymptotic techniques which have been developed for problems of turning-point type (Cole 1968, p. 125; O'Malley 1974, p. 168). The approach is based on the hypothesis that $\hat{\lambda}$ is large and negative for the present range of γ.

If we assume that $-\hat{\lambda} = \epsilon^{-2}$ for $\epsilon \to 0$ then a uniformly valid solution to (61) and (62), when $\gamma(\frac{1}{2}\pi) = O(\epsilon^{\frac{2}{3}})$, is

$$f \sim -\tan r - \pi\epsilon^{-\frac{2}{3}}[b(\epsilon)\,A_i(-\tilde{r}) + G_i(-\tilde{r}) + 1/\tilde{r}], \tag{64}$$

$$b(\epsilon) = \tan[(2/3\epsilon)\,(\gamma - \tfrac{1}{2}\pi)^{\frac{3}{2}} + \tfrac{1}{4}\pi], \tag{65}$$

$$\tilde{r} = \epsilon^{-\frac{2}{3}}(r - \tfrac{1}{2}\pi), \tag{66}$$

where A_i and G_i are standard functions (Abramowitz & Stegun 1965, pp. 446–450).

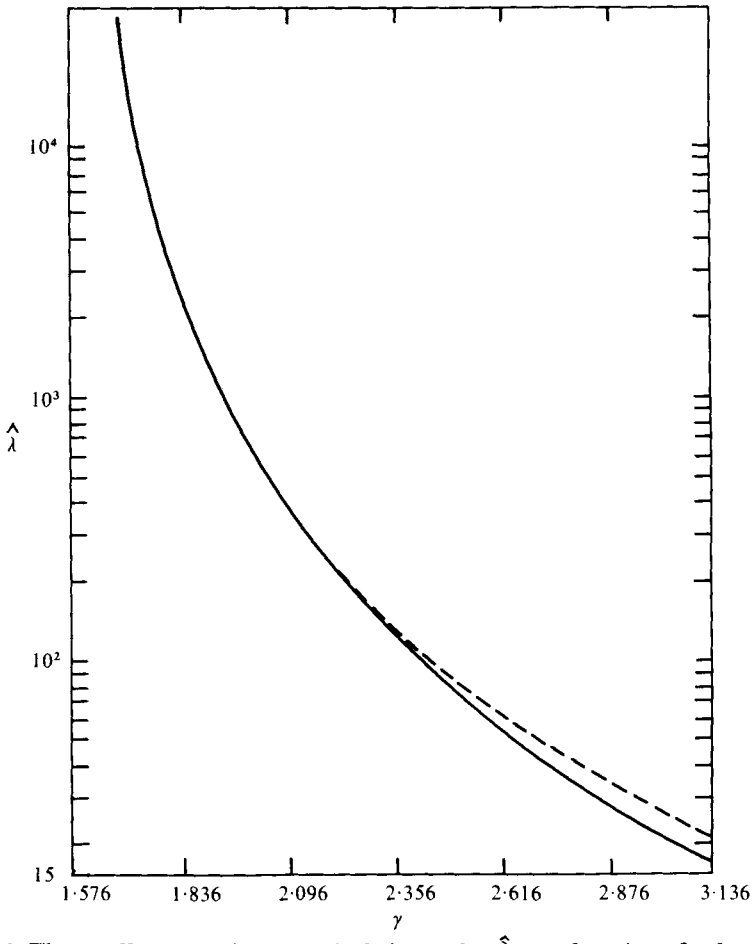

FIGURE 6. The smallest negative canonical eigenvalue $\hat{\lambda}$ as a function of γ for $\gamma > \frac{1}{2}\pi$. ——, asymptotic result; – – –, numerical result.

The integral condition (63) can be evaluated to show that

$$b \sim -\frac{\pi^{-1}}{2} \ln \frac{1+\sin\gamma}{1-\sin\gamma}. \tag{67}$$

The asymptotic values of the integrals of A_i and G_i were found in Luke (1962, p. 140). It follows from the definition of ϵ, (65) and (67) that

$$-\hat{\lambda}_n \sim \left[\frac{\frac{3}{2}(2n-\frac{1}{4})\pi - \tan^{-1}\left(\pi^{-1}\left[\frac{1+\sin\gamma}{1-\sin\gamma}\right]^{\frac{1}{2}}\right)}{(\gamma-\frac{1}{2}\pi)^{\frac{3}{2}}}\right]^2. \tag{68}$$

The smallest negative eigenvalue, found for $n = 1$, is plotted in figure 6 for a range of γ.

Numerical solutions were developed using a quasi-linearization approach where the initial guess is based on the analytical results in (64)–(68). Rapid convergence to the solution was obtained even for values of γ away from $\frac{1}{2}\pi$. The result for the eigenvalue

appears in figure 6. It may be observed that the analytical result, while formally valid for $\gamma \to \frac{1}{2}\pi$, is reasonably accurate (note the logarithmic scale for $\hat{\lambda}$) over a larger range of γ.

One may conclude from the results given here, (55) and (58), that the fully developed profiles are not spatially stable when $\gamma \geqslant \frac{1}{2}\pi$ and presumably could not be observed in an experiment. This result is not unlike that found by Chen & Libby (1968) in their study of the lower-branch solutions of the Falkner–Skan equations. The reverse flow profiles predicted by (52*a*) for $\gamma > \frac{1}{2}\pi$ are physically unrealistic.

One may inquire, with reason, about the predicted flow configuration when the physical dimensions of the system imply that $\gamma \to \frac{1}{2}\pi^-$. A study of fully developed flow in a three-dimensional, long, narrow vertical slab is described in the appendix. It is shown that the two-dimensional flow configuration cannot exist anywhere in the system when $\gamma \to \frac{1}{2}\pi^-$. At that value the profound influence of natural convection effects in the dimension transverse to the plane we have considered causes a three-dimensional configuration to appear.

6.2. *Numerical results*

Numerical solutions to (44)–(47) may be obtained when $0 < \gamma < \frac{1}{2}\pi$. The transformations

$$\hat{T}_0 = 1 - \tau z + \tau M \hat{\theta}, \quad \hat{\Psi}_0 = M\hat{\Psi}, \quad z = -1 + M\hat{z} \tag{69a,b,c}$$

are used in (44)–(47) to develop the canonical system

$$\hat{\Psi}_{\bar{y}\bar{y}} = \hat{\theta}_{\bar{y}}, \tag{70a}$$

$$\gamma^2[\hat{\Psi}_{\bar{y}}(-1+\hat{\theta}_{\hat{z}}) - \hat{\Psi}_{\hat{z}}\hat{\theta}_{\bar{y}}] = \hat{\theta}_{\bar{y}\bar{y}}, \tag{70b}$$

$$\hat{\Psi}(\hat{z}, \pm 1) = 1, \quad \hat{\theta}(\hat{z}, \pm 1) = 0, \tag{70c,d}$$

$$\hat{\Psi}(0, \bar{y}) = \bar{y}, \quad \hat{\theta}(0, \bar{y}) = 0. \tag{70e,f}$$

When $\hat{z} \ll 1$, a solution can be obtained in terms of a developing boundary layer adjacent to the wall and an accelerating core in a manner reminiscent of Schlichting's (1960, p. 149) calculation for Poiseuille flow. In order to avoid resolving the boundary layer in the numerical computation we use a Von Mises type transformation

$$w/M = \hat{w} = \hat{\Psi}_{\bar{y}} > 0 \tag{71a,b}$$

in (70). It follows that

$$\frac{\partial \hat{\theta}}{\partial \hat{z}} = \frac{1}{\gamma^2}\frac{\partial}{\partial \hat{\Psi}}\left(\hat{w}\frac{\partial \hat{\theta}}{\partial \hat{\Psi}}\right) + 1, \tag{72a}$$

$$\hat{w} = \hat{\theta} + f(\hat{z}), \tag{72b}$$

$$1 = \int_0^1 \frac{1}{\hat{\theta} + f(\hat{z})}\, d\hat{\Psi}. \tag{72c}$$

The condition $\hat{\Psi}_{\bar{y}} > 0$ is satisfied if no regions of reversed flow exist in the solution. Equation (72*b*) is a first integral of the momentum equation. The unknown function $f(\hat{z})$ remains to be found. Equation (72*c*) follows from the mass conservation condition

$$\int_0^1 \hat{w}(\bar{y}, \hat{z})\, d\bar{y} = 1.$$

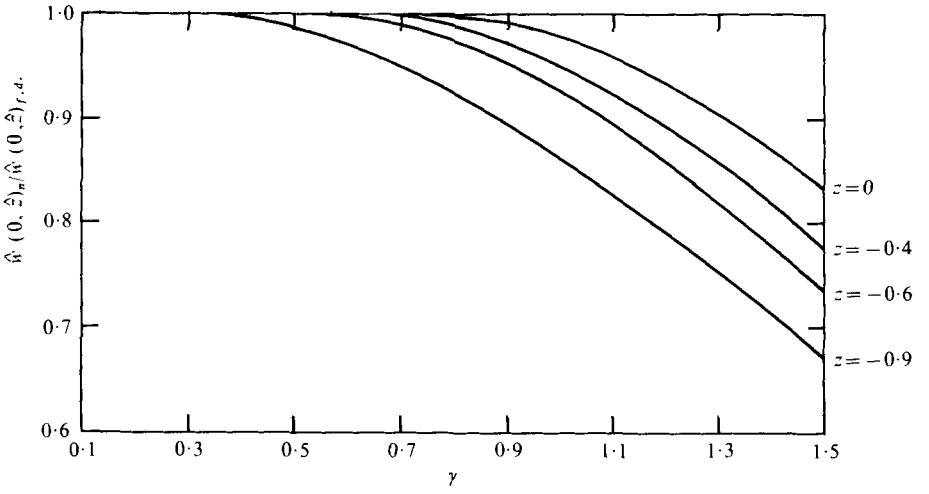

FIGURE 7. The ratio of the numerical value of the vertical centre-line velocity $\hat{w}(0,\hat{z})_n$ to the fully developed value $\hat{w}(0,\hat{z})_{f.d.}$ as a function of γ for several fixed depths in the slot.

Because of symmetry the boundary and initial conditions associated with (72) are taken to be

$$\hat{\theta}_{\hat{\Psi}}(\hat{z},0) = \hat{\theta}(\hat{z},1) = 0,$$

$$\hat{\theta}(0,\hat{\Psi}) = 0, \quad \hat{w}(0,\hat{\Psi}) = 1.$$

The parabolic equation (72a) was solved by the Crank–Nicolson difference scheme to determine $\hat{\theta}^{(n+1)}$ at $\hat{z} = (n+1)\Delta z$, with $\hat{w}$ evaluated at $(n+1)\Delta\hat{z}$. This required an inner iteration cycle in which (i) $\hat{\theta}^{(n+1)}$ is obtained from (72a), in which $\hat{w} = \hat{w}^{(n)}$, (ii) $f[(n+1)\Delta\hat{z}]$ is then found from (72c) and (iii) $\hat{w}^{(n+1)}$ is calculated from (72b) and compared with $\hat{w}$. The cycle is continued until

$$\max|\hat{w} - \hat{w}^{(n+1)}|/\max|\hat{w}^{(n+1)}| < 10^{-4}.$$

The solution for $f[(n+1)\Delta\hat{z}]$ in (72c) was found by Newton's method with $f(n\Delta\hat{z})$ as the initial guess. With $\Delta\hat{\Psi} = 0{\cdot}025$ and $\Delta\hat{z} = 0{\cdot}001$ the maximum number of inner iterations was two. The maximum number of iterations required to find $f[(n+1)\Delta z]$ was two.

The program was validated in two different ways. First, an invariant solution was obtained when the fully developed profiles

$$\hat{w}_{f.d.} = \frac{\gamma}{\sin\gamma}[1 - (\sin^2\gamma)\,\hat{\Psi}^2]^{\frac{1}{2}}, \tag{73a}$$

$$\hat{\theta}_{f.d.} = \hat{w}_{f.d.} - \gamma\cos\gamma/\sin\gamma \tag{73b}$$

were used as initial conditions. Then results obtained with the initial conditions (70e,f) were checked against the Schlichting-like asymptotic results for $\hat{z} \to 0$, with complete agreement. In the interest of brevity these details are omitted.

Figure 7 shows a plot of $\hat{w}(0,\hat{z})_n/\hat{w}_{f.d.}(0,\hat{z})$ as a function of γ for different values of z when $M = 1$. At a specific value of γ one can determine how close the flow is to the fully developed value at any value of z. For practical purposes when $\gamma \gtrsim 0{\cdot}85$ fully

developed flow is never achieved in the slot. Owing to the canonical form of $\hat{w}$ and the transformation in (69*c*) it should be clear that increasing M increases the deviation from fully developed flow at a specific z location. For a given slot configuration if the tube Rayleigh number (proportional to γ) is made sufficiently large a reasonable approximation to fully developed flow cannot be achieved in a slot of finite length. For $0 < M < 1$ additional parametric curves in figure 7 can be found. No new conclusions concerning fully developed flow are forthcoming.

7. Discussion and results

Two-dimensional flow dynamics in a conceptually plausible idealized model of a fault zone in the earth's crust have been elucidated. It has been hypothesized that the fracture zone can be represented by a tall, narrow, vertical slab of saturated porous media of arbitrarily large extent in the third dimension. The conclusions are restricted in their applicability by the assumptions of (i) mass input in the basement-rock section alone, (ii) no mass loss from the fault zone into the intersecting sediments, (iii) a free, open exit at the surface, (iv) compensating compaction and variable-viscosity effects, (v) the Boussinesq-type approximation for density variation, (vi) a wall temperature distribution increasing linearly with depth and (vii) no phase change (*in situ* boiling) of the liquid in the fault zone. None the less, the results obtained in the course of analysis can be used to develop, at the very least, a qualitative understanding of how liquid, heated at a large depth, is cooled as it rises towards the earth's surface in a region of relatively large vertical permeability. For the configuration examined one can ascertain the development of the flow pattern and temperature distribution as the system evolves towards the fully developed flow. It is clear that a two-dimensional model is not viable when the Rayleigh number based on the channel half-width, $Ry_e = \gamma R^{\frac{1}{2}}$, is sufficiently large. For instance, the theory predicts that if $R = 10^3$, $\gamma = \frac{1}{4}\pi$ and $L' = 3 \times 10^3$ m, for which the fault-zone width $2y_e' = 2\gamma R^{-\frac{1}{2}} L'$ is about 150 m, then two-dimensional flow will prevail with $Ry_e = 25$. However, if $2y_e' > 300$ m, then $\gamma > \frac{1}{2}\pi$, the slab looks more like a box and three-dimensional motion is possible. It may be noted from figure 7 and (69*c*) that in the former case the flow is within 7 % of fully developed even for $z = -0{\cdot}9$ ($M = 1$) whereas if $\gamma \approx \frac{1}{2}\pi^-$ and $Ry_e \approx 50$ then even for $z \to 0^-(M = 1)$ the flow is only within 17 % of fully developed. One may also observe that a two-dimensional flow configuration in a specific geological structure (specified y_e' and L') could be altered to a three-dimensional form by an increase in γ ($= R^{\frac{1}{2}} y_e$) associated either with a rise in R caused by enhanced thermal activity (larger τ) at a large depth or with additional fracturing due to tectonic activity (larger permeability). Both types of activity in the form of magma intrusions and/or seismic events are known to occur in geothermally active areas.

In figure 8 the temperature distribution with depth is characterized by the centre-line value $T(z, 0)$ for several values of γ when $M = \tau = 1$. Straight-line segments of the curves represent the fully developed regime. The remaining portions are obtained from the results of numerical computation. As γ is increased hotter liquid is brought up towards the surface. The centre-line temperature at $z = 0$ is shown in figure 9 as a function of γ. One may note that there can be substantial enhancement of this maximum temperature with respect to the boundary value.

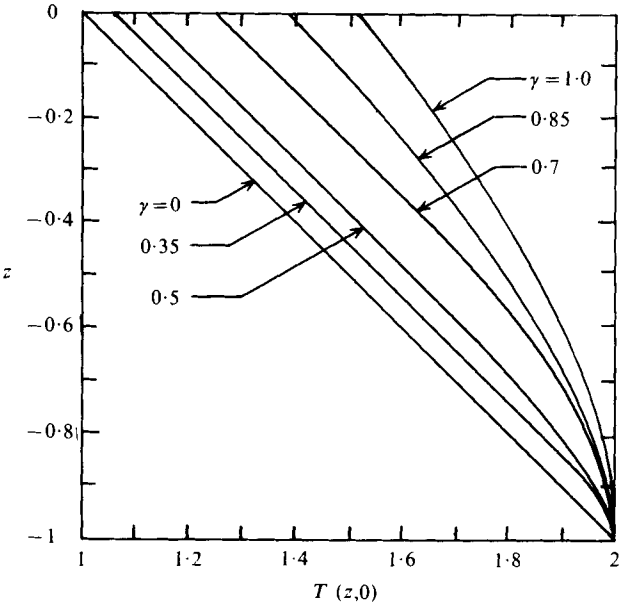

FIGURE 8. The centre-line temperature as a function of depth in the fault for several values of γ when $M = \tau = 1$.

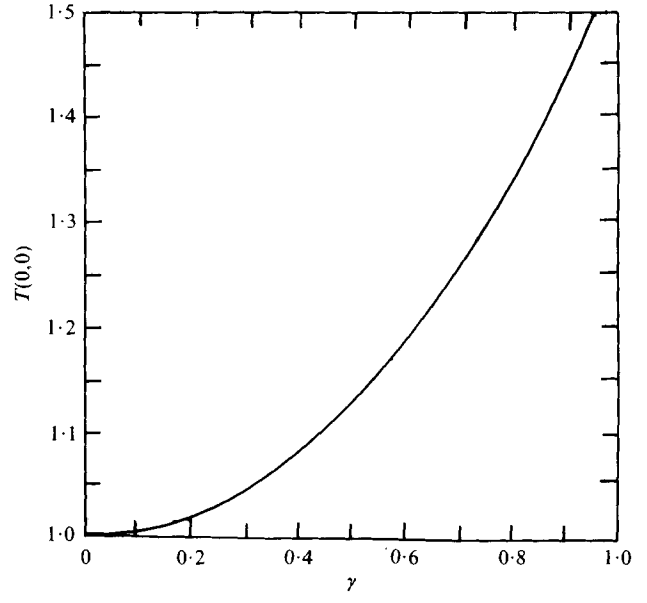

FIGURE 9. The centre-line temperature at $z = 0$ as a function of γ when $M = \tau = 1$.

The reference conductive vertical heat flux in the fault is defined by $Q'_R = \lambda'_m \Delta T'/L'$, where λ'_m is the thermal conductivity of the saturated medium. This quantity should be compared with the horizontal conductive flux through the walls into the neighbouring sediments, $Q'_w = -\lambda'_m(\partial T'/\partial y')(z, \pm y'_e)$, and with the convective heat transfer up the fault, $Q'_v = \rho' C'_v T' w'$. If we define the wall Nusselt number as $N_w = Q'_w/Q'_R$ then to a first approximation

$$N_w = (4\gamma^2 M\bar{z}/\pi y_e)^{\frac{1}{2}} \tag{74}$$

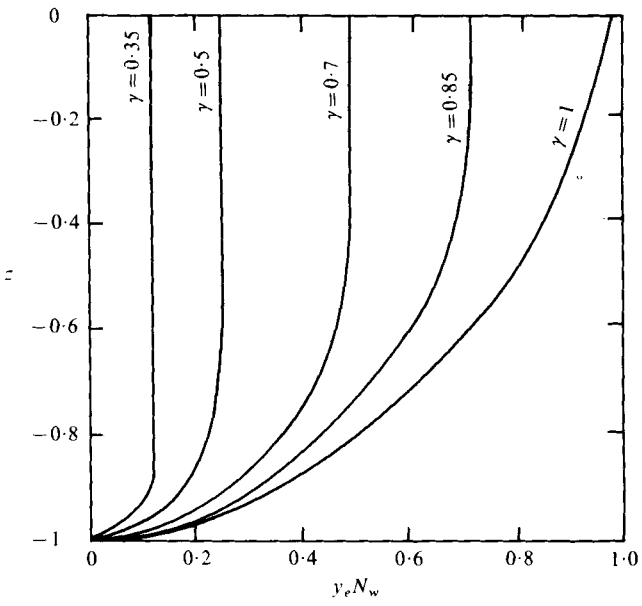

FIGURE 10. The reduced wall Nusselt number $y_e N_w$ as a function of depth in the fault for several values of γ when $M = \tau = 1$.

in the entry region while downstream we find

$$N_w = -\frac{1}{y_e} w(z, 1) \frac{\partial \hat{\theta}}{\partial \hat{\Psi}}(z, 1). \tag{75}$$

When fully developed flow is achieved then (73a, b) can be used in (75) to show that

$$N_{w\,\mathrm{f.d.}} = M\gamma^2/y_e. \tag{76}$$

In figure 10, $y_e N_w$ is plotted as a function of location in the slot. The curves were constructed from a combination of (74)–(76). Numerical results were used to evaluate (75). Vertical portions of the curves represent the fully developed flow regime. For a given fault-zone (slot) configuration, denoted by y_e, an increase in γ is related to that in $R^{\frac{1}{2}}$. The most important physical variation is associated with an increase in $\Delta T'$ and/or k'_0, the permeability.

Equations (74) and (75) imply that the heat transfer into the formation, arising from the convective flow process, is considerably larger than the vertical conductive flux. One would expect temperature distributions in these sediments to be controlled basically by heat flow from the neighbouring fault zone rather than by conduction from the basement.

The non-dimensional convective heat flux $Q'_v/Q'_R = (C'_v/C'_p)(R/\tau) wT$ implies that significant heat transfer in the system is associated with vertical convection.

A typical geophysical example can be constructed by considering a fault zone with the dimensions $y'_e = 100\,\mathrm{m}$ and $L' = 3\,\mathrm{km}$ in which the effective permeability $k'_0 = 10^{-9}\,\mathrm{cm}^2$. A temperature difference of 300 °C is specified with a boundary temperature at $z = 0$ of $T'_0 = 300\,^\circ\mathrm{K}$. Characteristic thermodynamic data based on T'_0 are used:

$$\alpha' = 2{\cdot}3 \times 10^{-4}\,^\circ\mathrm{C}^{-1}, \quad \nu'_0 = 9{\cdot}5 \times 10^{-3}\,\mathrm{cm}^2/\mathrm{s}.$$

It follows that the parameters characterizing the system have the values

$$y_e = 3{\cdot}33 \times 10^{-2}, \quad R = 2{\cdot}28 \times 10^{2}, \quad \gamma = 0{\cdot}50, \quad \tau = 1.$$

The characteristic vertical convection velocity $q'_R \approx 0{\cdot}62$ cm/day leads to a transport of mass $m' \approx 1{\cdot}22 \times 10^6$ kg/day along 1 km of the fault zone's horizontal extent when $M = 1$. The heat transfer associated with the mass transport can be evaluated from (74)–(76) along with the definitions of Q'_R, Q'_w and Q'_v. One finds that $Q'_R = 6{\cdot}5$ HFU (1 HFU $= 10^{-6}$ cal/cm^2 s) whereas the wall heat flux evaluated from the fully developed formula (76) is $Q'_w = 73$ HFU. For $\gamma = 0{\cdot}50$ the latter should prevail in the upper 70 % of the fault according to the results in figure 7. The associated convective heat flux in the fully developed section evaluated at the centre-line at $z = 0$ is $Q'_v = 3{\cdot}04 \times 10^3$ HFU, some 470 times larger than the reference conductive heat flux. These sample values reinforce the notion that the convection of heated water from a large depth, even at a rate of 1 cm/day, can transport significant quantities of mass and energy to the surface.

In a liquid-dominated geothermal system it is reasonable to expect that heated liquid rising in the fault zone will charge intersecting horizontal aquifers which have sufficient permeability. This mechanism can produce and maintain a reservoir of areal extent large compared with the fault-zone area itself. The heat flux through the surface above the fault and surrounding reservoir will be high compared with the background level of $1{\cdot}5 \times 10^{-6}$ cal/cm^2 s (Elders *et al.* 1972). Measurements at the East Mesa geothermal anomaly (Combs 1971) indicate that 5×10^6 cal/s cross about 110 km^2. If it is assumed that the originating mechanism of that energy is convection in a narrow fault zone then using order-of-magnitude estimates of the ratio Q'_v/Q'_R discussed earlier one can show that the horizontal area of the fault zone required is only about 3 km^2. Since the thermal activity of East Mesa extends along the Combs–Hadley fault for about 16 km this suggests an effective fault width of 200 m.

The solutions that have been developed for the stream function and temperature can be used in (2) to calculate the vertical pressure distribution in the system. In any section of the fault where the flow is nearly fully developed one can substitute (49) and (52) into (2) to produce the analogous pressure distribution

$$p = -\tfrac{1}{2}z^2 + M\gamma \cot \gamma |z|. \tag{77}$$

The variable p is defined in (4) as the non-dimensionalized difference between the actual pressure and the cold hydrostatic head $\rho'_0 g' z'$. The first term on the right-hand side of (77) describes the relative reduction in hydrostatic pressure associated with a linearized representation of the expansion of water with increasing temperature. Superimposed upon the resulting warm hydrostatic head is a pressure field, associated with the flow dynamics, which increases linearly with depth. In dimensional terms this quantity can be estimated from the value of the reference pressure p'_R in (4*e*), which is $O(10$ atm) in a typical geothermal environment if, in particular, $k'_0 = 10^{-9}$ cm^2. A measurement of the formation pressure distribution in a bore hole along with a temperature survey provides enough information to calculate the warm hydrostatic head and the net pressure difference at any depth. A basically linear increase in the difference with depth would provide some verification of the model considered in the present work. Reliable data of this sort are not at present available.

In future studies some of the restrictions mentioned above will be removed in order to model real geothermal systems more accurately. Perhaps the two most pressing points are the fault-zone charging process and loss of mass into the sedimentary aquifers that intersect the fault. Inclusion of the latter effect will permit a quantitative estimate of how the geothermal reservoir itself is supplied and maintained with hot water.

The authors would like to thank S. Datta, J. Foch and J. Gary for stimulating discussions concerning various aspects of the problem. The research was supported primarily by NSF AER 74-03429 AO2 and in part by funds from the Department of Energy through Lawrence Berkeley Laboratory.

Appendix

A fully developed solution to the three-dimensional analogue of (1)–(3) is sought in the rectangle $-1 \leqslant \bar{x} \leqslant 1$, $-1 \leqslant \bar{y} \leqslant 1$, where $\bar{x} = x/x_e$, $\bar{y}$ is defined in (15) and $x_e = x_e'/L'$ is the non-dimensional extent of the slot in the x' direction. On the bounding vertical surfaces the normal velocity vanishes and $T = 1 - \tau z$. The statement of global mass conservation analogous to (6) is

$$M = \frac{1}{4}\int_{-1}^{+1}\int_{-1}^{+1} w\, d\bar{x}\, d\bar{y}. \tag{A 1}$$

The problem is expressed in terms of the variables

$$u = v = 0, \quad w = w(\bar{x}, \bar{y}), \quad T = 1 - \tau z + \tau\theta(\bar{x}, \bar{y}), \tag{A 2a, b, c}$$

$$P'(z) = -(k+z), \quad w = k + \theta, \tag{A 3a, b}$$

$$\epsilon^2\theta_{\bar{x}\bar{x}} + \theta_{\bar{y}\bar{y}} + \gamma^2\theta = -\gamma^2 k, \tag{A 4}$$

$$\theta(\pm 1, \bar{y}) = \theta(\bar{x}, \pm 1) = 0, \quad M = \frac{1}{4}\int_{-1}^{+1}\int_{-1}^{+1} (k+\theta)\, d\bar{x}\, d\bar{y}, \tag{A 5a, b}$$

where u and v are transverse velocities, k is an integration constant and $\epsilon = y_e/x_e$. A general solution to (A 4) and (A 5) can be found in terms of an eigenfunction expansion. It follows from (A 3) and (A 5*b*) that when $\gamma < \pi$

$$w = k\left[\frac{\cos\gamma\bar{y}}{\cos\gamma} - 2\gamma^2 \sum_{n=0}^{\infty} \frac{(-1)^n \cosh(\bar{\beta}_n\bar{x}/\epsilon)\cos(\lambda_n y_e \bar{y})}{\lambda_n y_e \bar{\beta}_n^2 \cosh(\bar{\beta}_n/\epsilon)}\right], \tag{A 6}$$

$$M = \frac{k}{\gamma}\left[\tan\gamma - 2\epsilon\gamma^3 \sum_{n=0}^{\infty} \frac{\tanh(\bar{\beta}_n/\epsilon)}{(\lambda_n y_e)^2 \bar{\beta}_n^3}\right], \tag{A 7}$$

$$\bar{\beta}_n = [\tfrac{1}{4}(2n+1)^2\pi^2 - \gamma^2]^{\frac{1}{2}}, \quad \lambda_n y_e = \tfrac{1}{2}(2n+1)\pi. \tag{A 8}$$

In order to determine the conditions for which the two-dimensional profile, considered previously, is a viable representation of the flow in a three-dimensional region we consider asymptotic forms of (A 6) and (A 7) in the limit $\epsilon \to 0$.

(i) $0 < \gamma < \frac{1}{2}\pi$. If $\bar{\beta}_0$ is real and positive, then elementary asymptotics can be used to show that

$$w \approx \frac{\gamma M \cos\gamma\bar{y}}{\sin\gamma}(1 + O(\epsilon)) + O\left(\exp\left[-\bar{\beta}_0\frac{(1-|\bar{x}|)}{\epsilon}\right]\right). \tag{A 9}$$

The x dependence is confined to narrow boundary layers adjacent to $\bar{x} = \pm 1$. Thus the two-dimensional profile represented by the first term on the right-hand side is valid for $|\bar{x}| < 1$. The associated temperature profile, like that in (52*b*), can be found from (A 3), (A 9) and the asymptotic estimate $k = \gamma M/\tan\gamma + O(\epsilon)$. One may conclude that the fully developed flow in a tall, narrow, vertical slab containing a saturated porous medium will be basically two-dimensional if $\epsilon \ll 1$ and $\gamma < \frac{1}{2}\pi$ with the exception of narrow boundary layers at $\bar{x} = \pm 1$.

(ii) $\gamma \to \frac{1}{2}\pi^-$. It is evident from (A 9) that the asymptotic estimate fails when $\bar{\beta}_0 \to 0$, which occurs when $\gamma \to \frac{1}{2}\pi^-$. In fact a careful analysis indicates that the representation in (A 9) is valid only when $\gamma - \frac{1}{2}\pi \gg \epsilon^{\frac{2}{3}}$. In order to consider the flow when γ is very close to $\frac{1}{2}\pi$ the expression $\gamma = \frac{1}{2}\pi - \delta$, where $\delta \ll \epsilon^2$, is substituted into (A 6) and (A 7). The asymptotic analysis shows that the largest contribution from the first term in (A 7) is cancelled by the largest term arising from the first eigenvalue in the summation. It follows that, in the limit $\epsilon \to 0$, (A 7) reduces to

$$M = \frac{k}{\gamma}\left[\frac{\pi}{3\epsilon^2} + o(1)\right]. \tag{A 10}$$

A related cancellation process occurs in (A 6). When the asymptotic result and (A 10) are combined one finds the fully developed profile

$$w \sim \tfrac{3}{4}\pi M(1-\bar{x}^2)\cos\tfrac{1}{2}\pi\bar{y} + o(1). \tag{A 11}$$

We observe that the asymptotic estimate does not reduce to the two-dimensional profile anywhere in the rectangle. Rather one finds a parabolic distribution of the vertical velocity field in the x' direction. This result rationalizes the difficulties encountered with the two-dimensional spatial stability analysis in § 6.1 when $\gamma \to \frac{1}{2}\pi^-$.

REFERENCES

Abramowitz, M. & Stegun, I. A. 1965 *Handbook of Mathematics Functions*. Washington: Nat. Bur. Stand.

Bailey, R. A., Dalrymple, G. B. & Lanphere, M. A. 1976 *J. Geophys. Res.* **81**, 725.

Bailey, T. 1977 M.S. thesis, University of Colorado.

Black, H. 1975 M.S. thesis, University of Colorado.

Chen, K. K. & Libby, P. A. 1968 *J. Fluid Mech.* **33**, 283.

Cole, J. D. 1968 *Perturbation Methods in Applied Mathematics*. Blaisdell.

Combs, J. 1971 *Cooperative Geological–Geophysical–Geochemical Investigations of Geothermal Resources in the Imperial Valley of California*, pp. 5–27. University of California, Riverside.

Combs, J. & Hadley, D. M. 1977 *Geophysics* **42**, 17.

Donaldson, I. G. 1970 *Geothermics* **2**, 649.

Elders, W. A., Rex, R. W. & Meidav, T. 1972 *Science* **178**, 15.

Ellis, A. J. 1975 *Am. Sci.* **63**, 510.

Grindley, G. W. 1965 *N. Z. Geolog. Survey Bull.* **75**, 131.

Grindley, G. W. 1970 *Geothermics* **2**, 248.

Ince, E. L. 1956 *Ordinary Differential Equations*. Dover.

Kalaba, R. 1963 In *Nonlinear Differential Equations and Nonlinear Mechanics* (ed. J. P. Lasalle & S. Lefschetz), p. 97. Academic Press.

Landau, L. D. & Lifshitz, E. M. 1959 *Fluid Mechanics*. Pergamon.

Luke, Y. L. 1962 *Integrals of Bessel Functions*. McGraw-Hill.

Mercado, S. 1969 *Trans. Am. Geophys. Un.* **50**, 59.

O'Malley, R. 1974 *Introduction to Singular Perturbations*. Academic Press.

Rinehart, C. D. & Ross, D. C. 1964 *U.S. Geol. Survey Prof. Paper* no. 385, pp. 1–106.

Schlichting, H. 1960 *Boundary Layer Theory*, 4th edn. McGraw-Hill.

Swanberg, C. A. 1974 *Proc. Conf. Res. Development of Geothermal Energy Resources, Pasadena*, pp. 85–97.

Swanberg, C. A. 1976 *Proc. 2nd U.N. Symp. Development Use of Geothermal Resources, San Francisco*, vol. 2, pp. 1217–1229.

Van Dyke, M. 1964 *Perturbation Methods in Fluid Mechanics*. Academic Press.

Van Dyke, M. 1970 *J. Fluid Mech.* **44**, 813.

Ward, P. L. 1972 *Geothermics* **1**, 3.

White, D. E. 1961 *Proc. U.N. Conf. New Sources of Energy, Rome*, vol. 2, pp. 402–409.

Wu, F. T., Blatter, L. & Roberson, H. 1975 *Pageoph.* **113**, 87.